Graphitic C$_6$N$_6$-Based Copper Single Atom Catalyst Mimicking Adaptability of Nature for Dynamic Biosensors

Qing Hong, Hong Yang, Wang Li, Caixia Zhu, Yanfeng Fang, Sicheng Liang, Xuwen Cao, Yanfei Shen, Songqin Liu, Yuanjian Zhang*

Jiangsu Engineering Laboratory of Smart Carbon-Rich Materials and Device, Jiangsu Province Hi-Tech Key Laboratory for Bio-Medical Research, State Key Laboratory of Bioelectronics, School of Chemistry and Chemical Engineering, Medical School, Southeast University, Nanjing 211189, China, Email: Yuanjian.Zhang@seu.edu.cn

Abstract: Living systems can perceive and respond to environmental stimuli through multiple reaction pathways. Mimicking such adaptability from nature is highly envisioned in artificial intelligent chemical devices. However, the inconsistency of reaction conditions hampers the effective coupling of hybridized system with multiple reaction pathways. Herein, we reported a Cu$_{SA}$C$_6$N$_6$ single-atom catalyst with multiple oxygen-oriented reaction pathways that emerged as an intriguing way to address the challenges of conditions inconsistency. Cu$_{SA}$C$_6$N$_6$ could not only drive primary substrate oxidation with Cu-bound oxygen as intermediates but also undertake a second gain reaction under light stimuli, involving intermediates of free reactive oxygen species (ROS) under the same conditions. Notably, Cu$_{SA}$C$_6$N$_6$ demonstrated remarkable primary activity and a superb gain of up to 3.6 times under light stimuli. It was significantly higher by a factor of 80% than that under acknowledged temperature inducement with an increase of 30 ^{o}C from room temperature. As a proof-of-concept application, under light stimuli of different intensities, Cu$_{SA}$C$_6$N$_6$ was successfully applied to a single glucose sensor with adjustable sensitivity (5×10^{-6} - 6×10^{-3} M) and limit of detection (1.20-195.02 μM) precisely response to a diverse range of concentrations in vitro.

Keywords: carbon nitride, single atom catalysts, biomimetic, reaction adaptability, dynamic biosensors

Introduction

Establishment of indispensable adaptability plays a crucial role for living systems upon the wide variety of environmental stimuli. For instance, under normal conditions, thyroid hormones are primarily responsible for regulation of metabolism at basal level in human. Nonetheless, when we suddenly expose to the severe cold stimuli, the sympathetic nervous system would release high concentration of norepinephrine[1]. It significantly accelerates metabolism as the second pathway, which produce more heat to compensate cold. It features a primary activity in the normal state and a large gain in exceptional circumstances[2]. For the same reason, mimicking such adaptability from nature is highly envisioned in artificial intelligent devices, such as robots[3], brain-machine interface[4], and internet of things[5], to perceive freely between weak and strong signals, but remains a grand challenge. From a chemical point of view, construction of signal transduction units using stimuli-responsive catalysts with multiple reaction pathways would be a potential way to realize the basic activity and the gain effect. However, inconsistency of reaction conditions hampers the effective coupling of hybridized system[6].

As a polymeric semiconductor, carbon nitride has been intensively explored not only as a metal-free photocatalyst[7, 8] but also as a solid ligand to anchor single metal atom[9], owing to its engineerable conjugated repetitive units, rich lone pair electrons in skeleton, and high physicochemical stability. For example, carbon nitrides of different topological structures (e.g., C_3N_4, C_3N_2, C_5N_2 and C_2N)[10-13] and metal dopants (e.g., K and Cu)[14, 15] were developed for a wide range of photoredox reactions (e.g., clean water and sanitation)[16-18] and oxidase[19-21]/peroxidase-like[22-24] activities. It is worth noting that reactive oxygen-related intermediates participated the oxidation processes in both of these two types of reactions at similar conditions except for light stimuli.[25-28] As such, we reason that exploration of carbon nitrides with multiple oxygen-oriented reaction pathways would offer an intriguing way to address the forementioned challenges of conditions inconsistency in mimicking the adaptability from nature; however, to our

knowledge, it has been rarely reported yet.

Herein, we reported a copper single atom catalyst based on a highly conjugated carbon nitride ($Cu_{SA}C_6N_6$) in mimicking adaptability from nature. $Cu_{SA}C_6N_6$ could not only drove a basic substrate oxidation with Cu-bound oxygen as intermediates, but also undertake a second gain reaction under light stimuli, involving intermediates of free reactive oxygen species (ROS) under the same conditions. Interestingly, copper single atom participated these two reactions pathway but essentially as different roles, so synergistically did the C_6N_6 framework with a strengthened D-π-A charge transfer. As a result, $Cu_{SA}C_6N_6$ demonstrated conspicuous basic activity and a superb gain up to 3.6 times under light stimuli. It was significantly higher by a factor of 80% than that under acknowledged temperature inducement with an increase of 30 ℃ from room temperature, the maximum limit for most live that has ever endured. In a proof-of-concept application, under light stimuli of different intensity, $Cu_{SA}C_6N_6$ was successfully applied to a single glucose sensor with adaptable sensitivity and limit of detection, precisely response to a diverse range of concentrations in vitro.
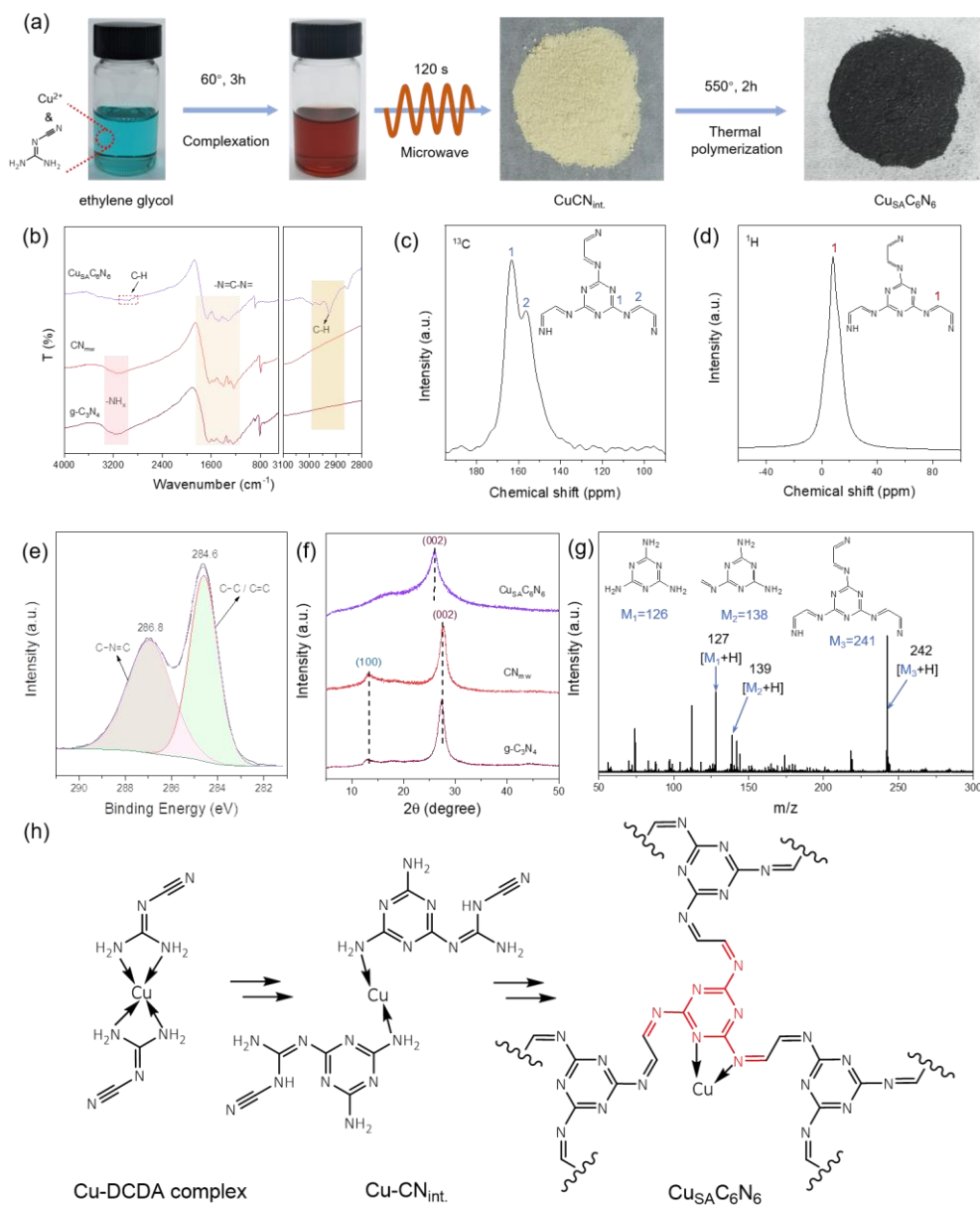
Fig. 1 Preparation and molecular structure of Cu$_{SA}$C$_6$N$_6$. (a) Brief synthesis procedures for Cu$_{SA}$C$_6$N$_6$. (b) FT-IR spectra of Cu$_{SA}$C$_6$N$_6$, CN$_{mw}$ and traditional g-C$_3$N$_4$. Solid-state (c) ^{13}C and (d) ^{1}H NMR spectra of Cu$_{SA}$C$_6$N$_6$. (e) C 1s XPS spectra of Cu$_{SA}$C$_6$N$_6$. (f) Normalized XRD patterns of Cu$_{SA}$C$_6$N$_6$, CN$_{mw}$ and traditional g-C$_3$N$_4$. (g) LDI-TOF mass spectrum of Cu$_{SA}$C$_6$N$_6$. (h) Proposed condensation processes and molecular structure for Cu$_{SA}$C$_6$N$_6$.

Results and Discussion

Synthesis and molecular structure of Cu$_{SA}$C$_6$N$_6$

As illustrated in **Fig. 1a**, copper acetate, which was selected as the Cu source, was first

complexed with dicyandiamide (DCDA) at 60 °C for 3 h to produce a reddish brown DCDA-Cu complex in ethylene glycol (EG). Then, a microwave-assisted condensation[18] using EG as the solvent was utilized for synthesizing the pale-yellow intermediate, donated as Cu-CN$_{int.}$, with a yield of 85%. Thanks to the pre-coordinated Cu-DCDA complex in EG, the possible formation of metal or metallic oxide in Cu-CN$_{int.}$ was avoided. As seen in **Fig. S1**, the X-ray diffraction (XRD) pattern of Cu-CN$_{int.}$ showed the only peak at 26.7°, assigning to an interlayer stacking. In contrast, the microwave-assisted polymerization of blue Cu^{2+} and DCDA mixture resulted in the product with additional XRD peaks for CuO, indicating the significance of pre-complexation in maintain the single atom state. The final product, Cu$_{SA}$C$_6$N$_6$, was obtained by further thermal polymerization at 550 °C. As control, CN$_{mw}$ were also fabricated by the same microwave-assisted polymerization of DCDA in EG without copper and subsequent thermal condensation.

It was worth noting that Cu$_{SA}$C$_6$N$_6$ was black, while the conventional g-C$_3$N$_4$ and CN$_{mw}$ was yellow. The combustion elemental analysis in **Table S1** showed a transformation of molar C/N value from Cu-CN$_{int.}$ of 0.73 to Cu$_{SA}$C$_6$N$_6$ of 0.95, approximate to 1. The FTIR spectrum was carried out to provide chemical structures of the new type of carbon nitride (**Fig. 1b**). It was observed that Cu$_{SA}$C$_6$N$_6$ showed strong vibration peaks around 800 and 1200-1700 cm^{-1}, assigning to the typical triazine rings (CN heterocycles). A characteristic peak around 2900 cm^{-1}, which was ascribed to the C-H stretching[29], was also observed. Those results implied Cu$_{SA}$C$_6$N$_6$ have a triazine core and non-cyclization linkers of -N=CH-.

The solid-state NMR provided further insights into the nature of the building blocks of Cu$_{SA}$C$_6$N$_6$. Two kinds of ^{13}C NMR signals were exhibited in the **Fig. 1c**, the conjugated triazine rings of Cu$_{SA}$C$_6$N$_6$ can be confirmed by the existence of carbon atoms in the triazine units, with a peak around 163 (1) ppm. Moreover, the ^{13}C signal for the second carbon atoms, which were indirectly connected to the triazine ring, was observed at adjacent chemical shifts at about 156 (2) ppm. Those two types carbon atoms were agreement with the FTIR spectrum of triazine rings and non-cyclization groups of -

5

N=CH-. Meanwhile, the ^{1}H magic angle spinning (MAS) NMR spectrum was also employed to gain local environment of H atom. As shown in **Fig. 1d**, the ^{1}H NMR spectrum of $Cu_{SA}C_6N_6$ exhibited a main characteristic peak around 8.3 ppm[30], ascribing to the -N=CH- group. Notably, this chemical shift of ^{1}H NMR spectrum was often assigned to aromatic carbon environment, indicating the existence of the triazine ring and the second conjugated carbon atom.

The high-resolution X-ray photoelectron spectroscopy (XPS) in **Fig. 1e** provided additional bonding information. The C1s XPS spectra exhibited two main peaks at 284.6 eV (C1) and 286.8 eV (C2), which were attributed to C-C peak and C species in triazine rings (C−N=C), respectively.[31] Interestingly, the carbon peak (ca. 284.6 eV) in $g\text{-}C_3N_4$ and CN_{mw} was assigned to random adventitious carbon, meanwhile the $C\text{-}(N)_3$ moved to high binding energy at 288.1 eV (**Fig. S2**). Those results demonstrated the non-cyclization group of -N=CH- was coupled, forming the -N=CH-CH=N- moieties in thermal polymerization process, in which the conjugated =CH-CH= linkage would promote the electron transfer in the C_6N_6 framework.

The crystalline texture of $Cu_{SA}C_6N_6$ was explored by XRD spectroscopy (**Fig. 1f**). As control samples, the XRD patterns of $g\text{-}C_3N_4$ and CN_{mw} were also measured. The $g\text{-}C_3N_4$ and CN_{mw} showed two characteristic peaks at 13.4° and 27.6°, corresponding to an in-plane structural packing motif (100) and an interlayer stacking reflection (002), respectively. While for $Cu_{SA}C_6N_6$, the diffraction peak at ca. 26.0° (002) was broadened and down-shifted, indicating a slightly enlarged interlayer spacing, which further supported the insertion of Cu atoms between C_6N_6 layers; meanwhile, the (100) peak is virtually invisible, suggesting a weakened crystallinity.

In order to verify the precise molecular structure of $Cu_{SA}C_6N_6$, the matrix-free laser desorption/ionization time-of-flight (LDI-TOF) mass spectra were measured. The m/z peaks were resulted from the ablation products of the repetitive C_6N_6 units in $Cu_{SA}C_6N_6$. **Fig. 1g** illustrated a series of m/z peaks including $[M + H^+]$ of 127.11 assigning to $C_3N_6H_6$ (M_1, melamine, calc.: 126), m/z $[M + H^+]$ of 139.15 attributable to $C_4N_6H_6$ (M_2,

calc.: 138), and m/z [M + H$^+$] of 242.15 attributable to $C_9N_9H_7$ (M$_3$, calc.: 241). Other m/z peaks, analyzed in **Fig. S3**, also supported the ablation unit's information. Therefore, all these structural explorations demonstrated the Cu$_{SA}$C$_6$N$_6$ featured a repetitive basic triazine core and a -N=CH--CH=N- linkers. The possible condensation processes and molecular structure of Cu$_{SA}$C$_6$N$_6$ were proposed in **Fig. 1h**.
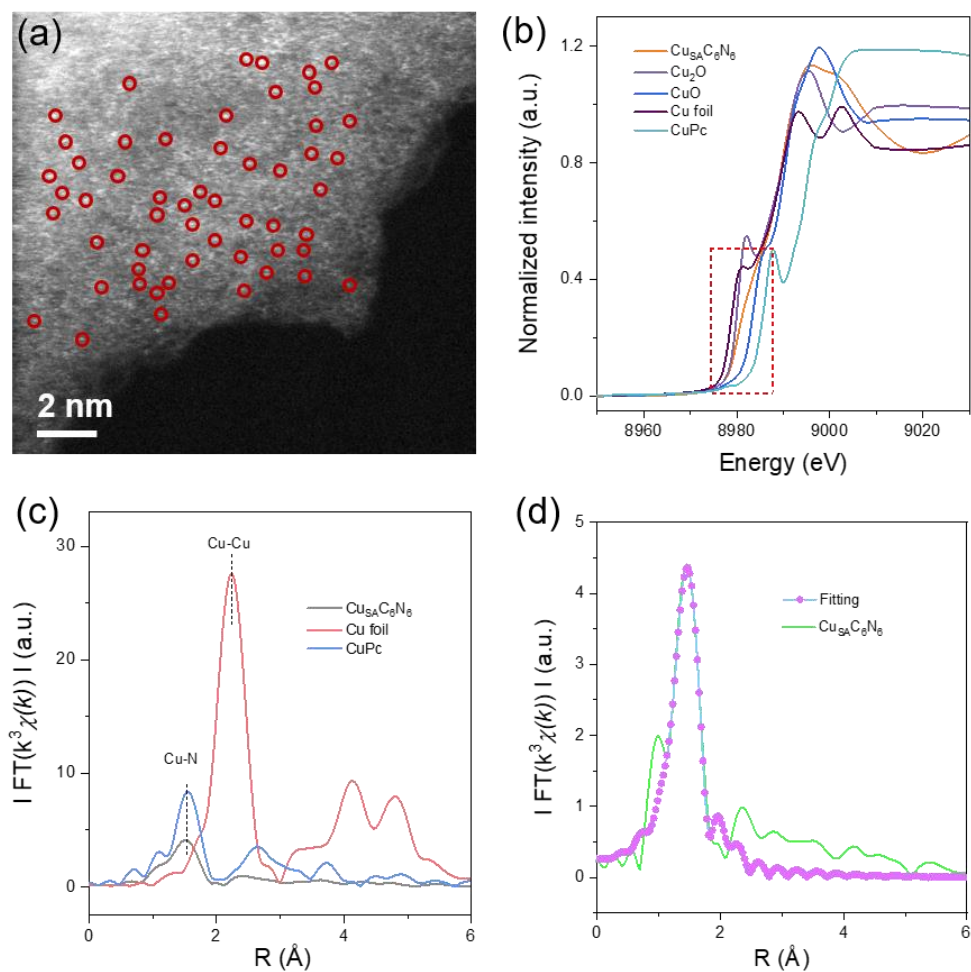
Fig. 2 Morphologies and Synchrotron XAFS measurements of Cu$_{SA}$C$_6$N$_6$. (a) HAADF-TEM image of Cu$_{SA}$C$_6$N$_6$. (b) Cu k-edge XANES profiles of Cu foil, Cu$_2$O, CuO, Cu$_{SA}$C$_6$N$_6$ and CuPc. (c) Cu k-edge EXAFS spectra in R-space of Cu$_{SA}$C$_6$N$_6$, CuPc, and Cu foil samples. (d) EXAFS fitting curve for Cu$_{SA}$C$_6$N$_6$ in R-space.

Cu single-atom structure of Cu$_{SA}$C$_6$N$_6$

The scanning electron microscopy (SEM) images in **Fig. S4a** showed the disordered and porous structure of Cu$_{SA}$C$_6$N$_6$, distinguishing from a blocky structure of g-C$_3$N$_4$

and CN_{mw} (**Fig. S4b and c**). The high-resolution TEM images in **Fig. S5** showed the $Cu_{SA}C_6N_6$ exhibited an ultrathin nanosheet-like morphology and no obvious Cu/CuO nanoparticles were observed on the surface of C_6N_6 framework, which were agreement with the XRD results. The large-area high-angle annular dark-field scanning transmission electron microscopy (HAADF-STEM) image (**Fig. 2a**) confirmed that Cu existed as single atoms and emerged as abundant isolated bright spots which were uniformly dispersed on the C_6N_6 matrix highlighted by a red circle. The high Cu content in $Cu_{SA}C_6N_6$ was quantitatively measured by inductively coupled plasma mass spectrometer (ICP-MS) to be ~2.36 wt %. The corresponding STEM-EDS elemental mapping images exhibit that C, N, O and Cu species are atomically and homogeneously dispersed across the whole C_6N_6 nanosheet (**Fig. S6**).

To further investigate chemical state and local coordination environment of Cu species in $Cu_{SA}C_6N_6$, X-ray absorption fine structure (XAFS) measurements of the Cu K-edge were performed. As control samples, the XAFS patterns of Cu foil, Cu_2O, CuO and CuPC were also measured. From the normalized Cu K-edge X-ray absorption near edge structure (XANES) spectra (**Fig. 2b**), the absorption edge of $Cu_{SA}C_6N_6$ was located between those for Cu_2O and CuO, indicating that the coexistence of Cu^+ (which acted as a predominant oxidation state)[32] and Cu^{2+} carried a partial positive charge between 0 and +2. Meanwhile, the related FT k^3-weighted EXAFS spectrum in R space for $Cu_{SA}C_6N_6$ was also measured (**Fig. 2c**). The presence of characteristic peak located at 1.51 Å indicated the first coordination shell of Cu-N. Furthermore, there was no obvious metallic Cu-Cu interaction at around 2.2 Å, demonstrating that Cu atoms were atomically dispersed in the $Cu_{SA}C_6N_6$ matrix. This result was further corresponding with the HAADF-STEM images. To further explore the atomic coordination of Cu, the related FT k^3-weighted EXAFS fitting in R-spaces (**Fig. 2d**) was performed to reveal the detailed structural information. The fitting analysis result (**Table S2**) showed that the average Cu-N coordination number in the first coordination shell was 2.0 and the Cu-N bond length was 1.93 Å, indicating one Cu atom was coordinated by two N atoms forming a $Cu-N_2$ moiety.

The existence of the Cu-N chemical bonding information was also verified by the N1s and Cu2p XPS spectra. As shown in **Fig. S7**, the N1s peak could be deconvoluted into four peaks, in which the dominant N species around 398.0 eV was mainly ascribed to the formation of pyridinic nitrogen (C=N-C) in triazine rings; The peak at 399.7 eV and 400.7 eV were corresponding to pyrrolic N and graphitic N. Interestingly, a new bond at 398.7 eV was observed, demonstrating the formation of a Cu-N bond, which was also in agreement with the EXAFS spectrum in R space measurements (**Fig. 2c**). The Cu 2p spectrum (**Fig. S8**) exhibited two main peaks with binding energy at 932.9 and 952.9 eV, which were assigned to Cu $2p^{3/2}$ and Cu $2p^{1/2}$, respectively. Furthermore, the weak satellite peak was recorded at 944.8 eV, indicating the presence of Cu^{2+} species in $Cu_{SA}C_6N_6$. The spectrum for Cu $2p^{3/2}$ could be deconvoluted into two peaks at 932.6 and 934.8 eV, corresponding to Cu^{1+} and Cu^{2+}, respectively.[33, 34] This result further proved the coexistence of Cu^+ and Cu^{2+} in $Cu_{SA}C_6N_6$, consisting with the XANES spectroscopy (**Fig. 2b**).

Basic catalytic activity and Gain effect of $Cu_{SA}C_6N_6$

The specific transition Cu-N coordination filled into C_6N_6 framework and endowed it a peroxidase-like catalytic activity, which was evaluated by catalytic oxidation of 2, 2'-azino-bis (3-ethylbenzothiazoline-6-sulfonic acid) (ABTS) in the presence of H_2O_2 (**Fig. 3a and Fig. S9**). Meanwhile, the catalytic activity of $Cu_{SA}C_6N_6$ was optimized according to various Cu contents (**Fig. S10**). In order to realize the gain effect, the acknowledged temperature inducement was firstly explored. As shown in **Fig. 3b and S11**, the peroxidase-like activity of $Cu_{SA}C_6N_6$ showed elevated velocity with the serious of temperatures. It was observed that when the temperature increased from room temperature (25 °C) to as high as 55 °C, the catalytic activity only reached 2 times of the original one.

Owing to the π-conjugated hybridization of energy levels along polymer linker and π-stacking between linkers, $Cu_{SA}C_6N_6$ demonstrated a narrow optical gap (1.30 eV, **Fig. S12**). It had a wide absorbance in ultraviolet-visible-near-infrared regions (**Fig. S13**),

differing from most polymeric carbon nitrides. Thus, $Cu_{SA}C_6N_6$ was able to effectively utilize lower excitation energy of light to enhance photocatalytic activity. Interestingly, when irradiated by a household white LED lamp (400-900 nm, 50 mW/cm^2, **Fig. S14**), the color of ABTS$_{ox}$ turned into dark green, indicating a considerable enhancement in the peroxidase-like activity of $Cu_{SA}C_6N_6$. **Fig. 3c** shows the UV-vis absorbance of ABTS after catalytic oxidation in the presence of H_2O_2 measured under different reaction conditions. The quantitative absorbance of ABTS$_{ox}$ (**Fig. 3c)** at 417 nm under light irradiance (0.72) was 3.6 times of that in the dark (0.20). This result was equivalent of an improved total peroxidase-like rate constant of 3.4 times (**Fig. S15**). A series of control experiments, including examination of oxidase-like activity of $Cu_{SA}C_6N_6$, direct photocatalytic oxidation of ABTS and decomposition of H_2O_2, were also undertaken, which excluded the potential interferences for the profound gain of peroxidase-like activity (**Fig. S16**). Moreover, as an intrinsic advantage, the photocatalytic processes by $Cu_{SA}C_6N_6$ could been facilely modulated via tuning the irradiation power density (**Fig. S17**).

The intrinsic enhancement mechanism of peroxidase-like activity of $Cu_{SA}C_6N_6$ under light stimuli was further investigated. In the first set of experiments, to exclude photothermal effect, the temperature of the reactor after irradiation using the LED lamp was measured. It was found that the irradiation for 10 min made the temperature only improve 3 °C (**Fig. S18)**, while the practical reaction in this study only took 3 minutes, indicating an even smaller temperature fluctuation. The enhancement of peroxidase-like activity under such minor increase of temperature was further measured (Fig. **S19 and S20**), confirming the photothermal-induced gain effect here was marginal.
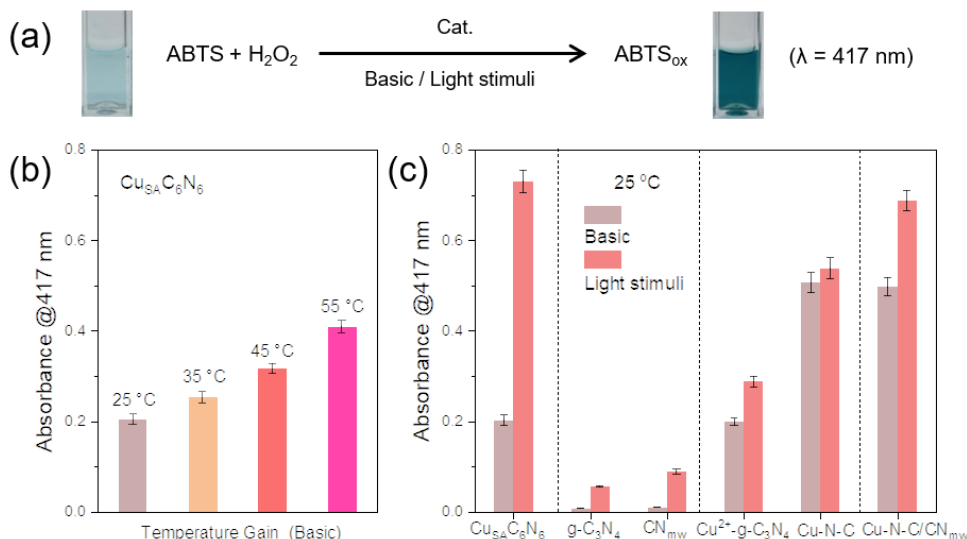
Fig. 3 Gain effect evaluation by the standard ABTS catalytic oxidation. (a) Equation and photos of standard ABTS catalytic oxidation. (b) Absorbance of $ABTS_{ox}$ catalyzed by $Cu_{SA}C_6N_6$ under different temperature. (c) Absorbance of $ABTS_{ox}$ catalyzed by $Cu_{SA}C_6N_6$, g-C_3N_4, CN_{mw}, Cu^{2+}-g-C_3N_4, Cu-N-C and Cu-N-C/CN_{mw} with and without light stimuli.

In contrast to $Cu_{SA}C_6N_6$, the basic catalytic activity of the control g-C_3N_4 and CN_{mw} was negligible (**Fig. 3c**). Under light stimuli, the catalytic activities of them were enhanced, indicative of typical photocatalysts, but still much lower than that of $Cu_{SA}C_6N_6$. In order to further understand the excellent basic activity and gain effect of $Cu_{SA}C_6N_6$, two well-known copper-containing nanozymes, i.e., Cu^{2+}-g-C_3N_4 and Cu-N-C with the similar Cu-N coordination with were also preprepared. Interestingly, although a higher basic activity of Cu^{2+}-g-C_3N_4 and Cu-N-C were observed (**Fig. 3c**), none of them demonstrated the similar large gain effect like $Cu_{SA}C_6N_6$ under light stimuli, indicating the second reaction pathway was not effectively opened. For the former, although charge separation would occur in C_3N_4 framework under light irradiation, Cu ions quenched it as the recombination sites. For the latter, the graphitic carbon framework had an intrinsic poor charge separation ability. Those results indicated that most conventional catalysts were only applicable to effectively drive a single enzyme-like or photocatalytic reaction, because of inconsistency of requirements for basic and gain reactions. It was supposed that the unique conjugated linkers (-

N=CH-CH=N-) not only elongated the distance of D-A to reduce recombination at Cu sites but also simultaneously compensated the charge transfer between D-A in $Cu_{SA}C_6N_6$, leading to synergistic two-pathway catalytic reaction.

As more controls, two highly efficient enzyme-like catalyst and photocatalyst, namely Cu-N-C and CN_{mw}, were mixed into a nanocomposite (Cu-N-C/CN_{mw}, **Fig. S21 and 22**). As shown in **Fig. 3c**, Cu-N-C/CN_{mw} indeed realized a gain effect under light stimuli, however, which reached only approximately one third of that by $Cu_{SA}C_6N_6$. A series of characterizations, including electrochemical impedance spectra (EIS, **Fig. S23**), photoluminescent spectra (PL, **Fig. S24**) and photoelectrochemical measurements (PEC, **Fig. S25**) of $g-C_3N_4$, Cu-N-C/CN_{mw} and $Cu_{SA}C_6N_6$ demonstrated the faster velocity of intramolecular charge migration in C_6N_6 matrix in comparison with that at the interface of Cu-N-C and CN_{mw} played the crucial role in the boosted gain effect.

Synergistic basic and gain reactions mechanism of $Cu_{SA}C_6N_6$

To understand the basic and gain reaction mechanism of $Cu_{SA}C_6N_6$ in peroxidase-like activity under light stimuli, the possible intermediate reactive species were first studied using the scavenger trapping experiments. As illustrated in **Fig. S26**, both superoxide dismutase (SOD) and isopropanol, corresponding to the superoxide ($O_2^{\cdot-}$) and hydroxyl radicals ($\cdot OH$) scavengers, respectively, had negligible influences on the oxidation of ABTS catalyzed by $Cu_{SA}C_6N_6$, indicating no formation of these two radicals during the activation of H_2O_2. Nevertheless, the catalytic activity was noteworthily restrained when isopropanol was added into the same reaction solution under light stimuli (**Fig. S27**), indicating that the redox of H_2O_2 generated the $\cdot OH$ as a major step in the $Cu_{SA}C_6N_6$ catalyzed ABTS oxidation. Other radical probes (**Fig. S28 and S29**), such as nitrotetrazolium blue chloride (NBT) and coumarin, and electron spin resonance (ESR) spectra (**Fig. 4a, b**) also supported this speculation. For instance, there were no ESR signal for any ROS-trapping agent adduct, reminiscent to the case catalyzed by HRP. Interestingly, under light stimuli, the typical characteristic peak of DMPO-·OH spin

adduct with the typical signal intensity of 1:2:2:1 was observed in **Fig. 4b**, indicating the existence of ·OH, in agreement with the scavenger trapping experiments in **Fig. 4b**.
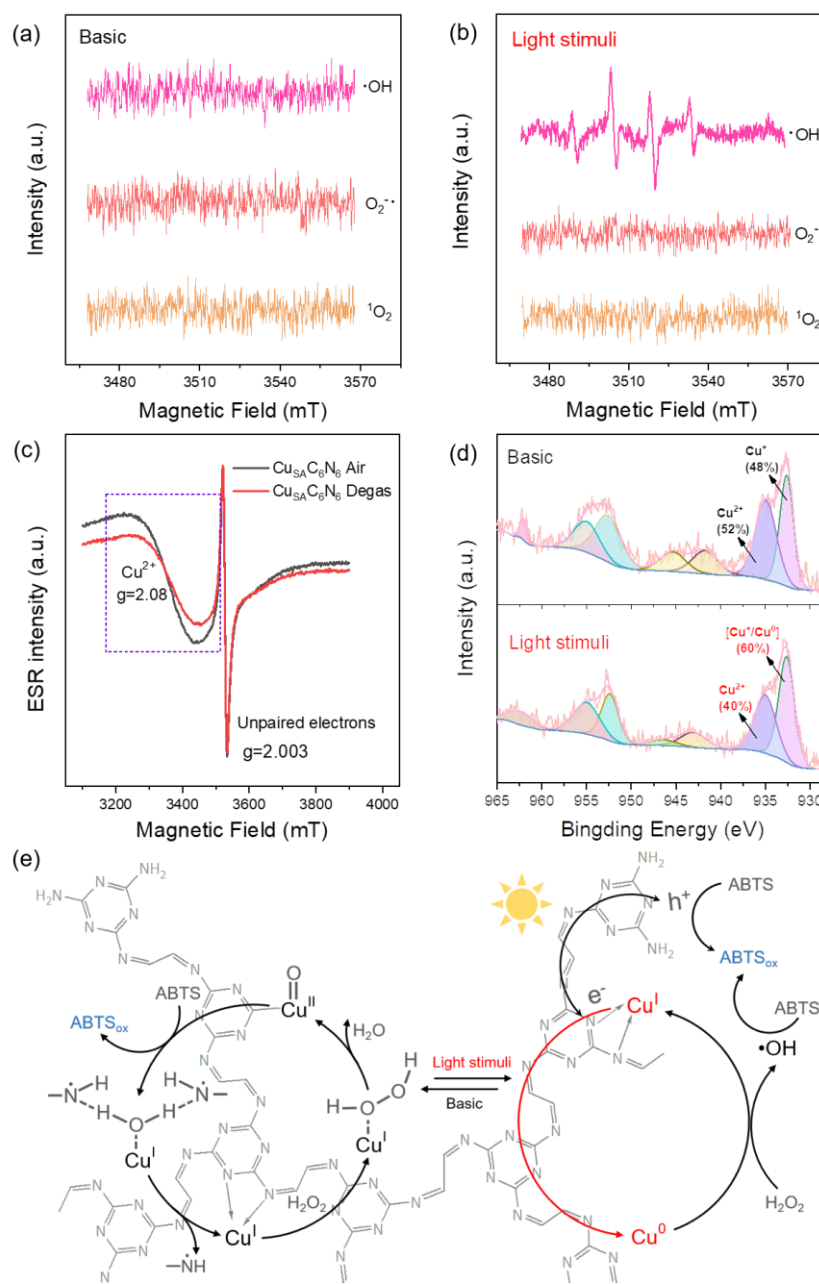
Fig. 4 Basic and gain reactions mechanism of $Cu_{SA}C_6N_6$. ESR spectra of the spin adduct of ·OH, $O_2^{·-}$, $^1O_2$ generated during the activation of H_2O_2 by $Cu_{SA}C_6N_6$ in 0.2 M HAc-NaAc (pH 5.0) under the (a) basic and (b) gain reactions. (c) EPR spectra of $Cu_{SA}C_6N_6$ in air and after degassing at 200 °C in vacuum for 12 h. (d) XPS spectra of dynamic changes of valence state of $Cu_{SA}C_6N_6$ under the light on and off state. (e) Proposed mechanism for dual peroxidase-like and photocatalytic pathways in mimicking the basic activity and the gain effect by using $Cu_{SA}C_6N_6$.

The solid-state ESR signal of $Cu_{SA}C_6N_6$ (**Fig. 4c**) further demonstrated the probability of the formation of Cu=O species during the peroxidase-like reaction. Given Cu had a much stronger ESR intensity in air than in degassed conditions at g of 2.08, it was speculated that $Cu_{SA}C_6N_6$ might have a similar catalytic mechanism to HRP via a bound ROS pathway.[26] Meanwhile, in order to investigate the charge transfer as well as chemical-bond evolution of $Cu_{SA}C_6N_6$ under light irradiation, the synchronous illumination X-ray photoelectron spectroscopy (SI-XPS) technique[35] was employed to clarify the dynamic changes of Cu-N. As shown in **Fig. 4d**, the spectrum for Cu $2p^{3/2}$ was deconvoluted into two peaks at 932.6 and 934.8 eV, which were assigned to Cu^{1+} and Cu^{2+}, respectively. Interestingly, the percentage of Cu^{2+} decreased from 52% in the dark to 40% under light stimuli, meanwhile the percentage of Cu^{1+} and Cu^0 increased from 48% to 60%, supporting the acceptance of electrons for Cu atoms in the gain reaction.[36] Besides, as a significant Cu^{2+} was still retained under light stimuli, the basic reaction pathway should also be activated during the gain reaction performed, but the latter was much more efficient.
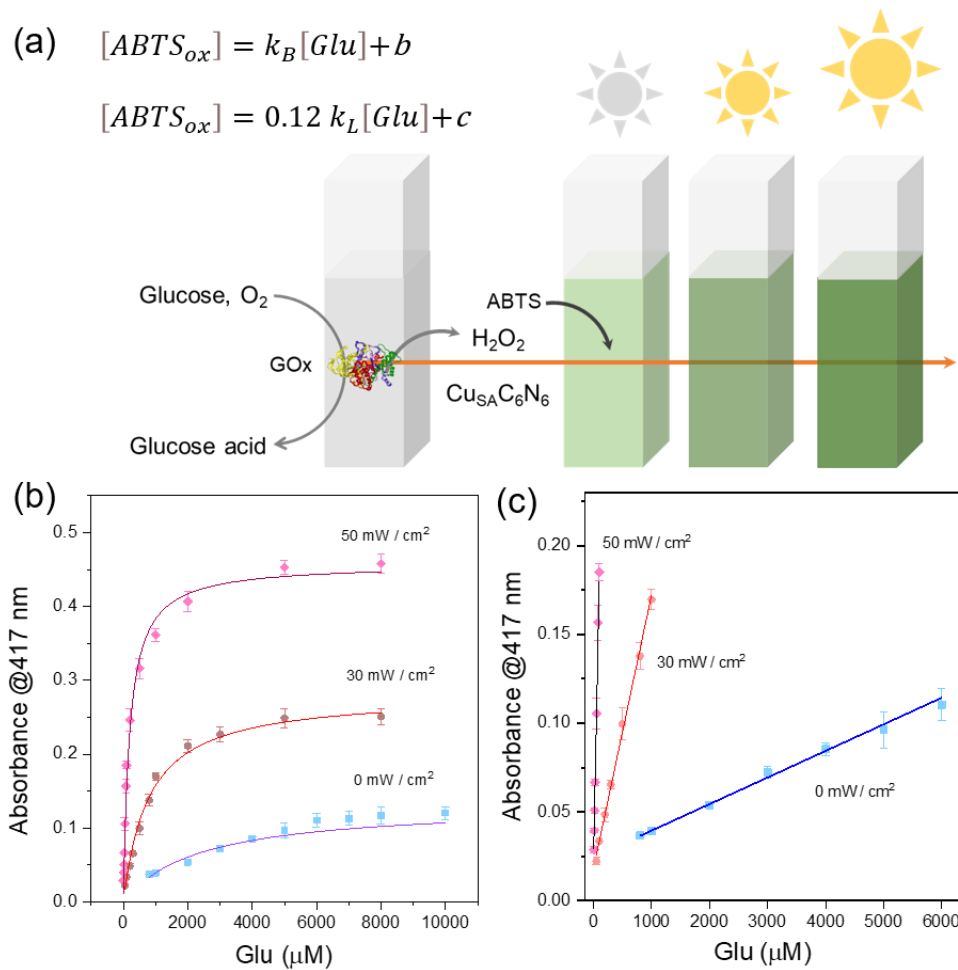
Taking all these experimental evidences into consideration, the mechanism for the light-gained peroxidase-like catalytic activity of $Cu_{SA}C_6N_6$ was proposed (**Fig. 4e**). Briefly, in the basic reaction without light irradiation, H_2O_2 firstly bound to the N-coordinated metal site of Cu^I in $Cu_{SA}C_6N_6$ to form the Cu^I-superoxo species. Then, O-O cleavage occurred to decompose the adsorbed H_2O_2 into H_2O upon the oxidation of Cu^I to Cu^{II}=O. Next, the Cu^{II}=O was reduced by the ABTS substrate owing to the affinity of ABTS on Cu^{II}=O and the electron-donor ability of ABTS. In contrast, when the light was on, the photocatalytic processes were activated, which provided a new pathway to enhance the catalytic activity. The terminal mixed-valence Cu species emerged as collectors of the photogenerated electrons, then these photoelectrons reduced Cu^+ to Cu^0, subsequently. After that, Cu^0 contributed to the in-situ decomposition of H_2O_2 to produce ·OH via Fenton-like process.[37] Finally, H_2O_2 oxidized Cu^0 to promote the formation of Cu^+ species, completing the photocatalytic cycle and maintain the mixed valence states.

Those aforementioned results further demonstrated that $Cu_{SA}C_6N_6$ not only had a

peroxidase-like Cu-N coordination active center but also owned an unusual donor-π-acceptor (D-π-A) structure (**Fig. 1h**), where the single Cu atom acted as electron acceptors, the triazine rings emerged as electron donors (photovoltaic center), and the -N=CH-CH=N- linkers offered π-conjugated charge transfer channels for D-A couples. Those π-interconnected D-A couples played a crucial role in addressing inconsistency of requirements for basic and gain reactions by not only reducing recombination (control sample: Cu^{2+}-g-C_3N_4) and promoting the charge separation (control sample: Cu-N-C) but also accelerating intramolecular charge transfer (control sample: Cu-N-C/CN_{mw}). Those results indicated that $Cu_{SA}C_6N_6$ had more intramolecular charge transfer feature from the triazine rings unit to Cu atom than Cu^{2+}-g-C_3N_4 upon light stimuli.

Adaptable sensing of H_2O_2 and Glucose

Improving the quality of life is an enduring topic in the modern society. For this, the intelligent response of glucose has received increasing attention, as a powerful tool in the field of human health. Recent years, many biosensing methods for detecting glucose based on nanozymes have found broad utility due to its simplicity, sensitivity, and high selectivity. Despite enormous advances, in vitro recording the narrow linear concentration range of glucose cannot directly provide physiological information for better comprehending dynamic fluctuation of glucose in brain.[38] Intelligent response to glucose with a random concentration range at a single sensing interface in vivo is highly envisioned to understand the pathological process, but still facing great challenges.

(a)
$$[ABTS_{ox}] = k_B[Glu] + b$$
$$[ABTS_{ox}] = 0.12\, k_L[Glu] + c$$

(b) Absorbance @417 nm vs Glu (μM); 50 mW / cm², 30 mW / cm², 0 mW / cm²

(c) Absorbance @417 nm vs Glu (μM); 50 mW / cm², 30 mW / cm², 0 mW / cm²

Fig. 5 (a) Principle of adaptable sensing of Glucose based on $Cu_{SA}C_6N_6$, (b) Absorbance of $ABTS_{ox}$ catalyzed by $Cu_{SA}C_6N_6$ with different concentration of glucose in the presence of glucose oxidase under light stimuli of tuned intensity.

As a proof of the concept, we proposed an intelligent response sensor for monitoring the glucose in vitro (**Fig. 5a**). In principle, the accurate linearity can be used only if the calibration function is linear[39], e.g., a low concentration range, in which, the v is proportional to the first-order with glucose (**Eq. in Fig. 5a inset and SI**). But at high concentration rage, the absorbance reached a plateau, leading to a narrow detection range. Relating response with analyte concentrations at logarithmic scale primarily considering linear fitting coefficient of determination (R^2) is widely used, but is questioned in uncertainness very recently[40]. Developing adaptive sensitivity and linear detection concentration range using the real kinetic equations is an ideal solution to obtain a full-scale linear detection range. As shown in **Fig. 5c**, the sensor provided three

orders of magnitude linear range with increase of irradiation power density. Concretely, without light irradiance, glucose could be detected with a linear range at 8×10^{-4} - 6×10^{-3} M, while the linear range can be extended downward from 5×10^{-5} - 1×10^{-3} M at 30 mW/cm^2 to 5×10^{-6} - 6×10^{-5} M at 50 mW/cm^2. At the same manner, the limit of detection (LOD) for glucose was tuned from 195.02 μM in the dark, to 15.07 μM and 1.20 μM under irradiation at 30 and 50 mW/cm^2, respectively. In this sense, owing to the high adaptability of Cu$_{SA}$C$_6$N$_6$ along with the intrinsic outstanding temporal and spatial resolution of light stimuli, this intelligent response sensor would supply a prospective candidate for dynamic analysis for intelligent artificial devices, such as robots, brain-machine interface, and internet-to-things in the future.

Conclusion

In summary, we proposed a Cu$_{SA}$C$_6$N$_6$ single atom catalyst with a highly conjugated carbon nitride that addressed inconsistency of requirements for basic and gain reactions in mimicking the adaptability from nature. All of structural explorations demonstrated Cu$_{SA}$C$_6$N$_6$ featured a repetitive basic triazine core and a -N=CH--CH=N- linkers, endowing Cu$_{SA}$C$_6$N$_6$ with a peroxidase-like Cu-N coordination active center an unusual donor-π-acceptor (D-π-A) structure. Accordingly, Cu$_{SA}$C$_6$N$_6$ could not only drove a basic substrate oxidation with Cu-bound oxygen as intermediates, but also undertake a second gain reaction under light stimuli, involving intermediates of free reactive oxygen species (ROS) under the same conditions. Interestingly, copper single atom participated these two reactions pathway but essentially as different roles, so synergistically did the C$_6$N$_6$ framework with a strengthened D-π-A charge transfer. As a result, Cu$_{SA}$C$_6$N$_6$ demonstrated conspicuous basic activity and a superb gain up to 3.6 times under light stimuli. It was significantly higher by a factor of 80% than that under acknowledged temperature inducement with an increase of 30 °C from room temperature. Meanwhile, under light stimuli of different intensity, Cu$_{SA}$C$_6$N$_6$ was successfully applied in intelligent response of glucose with adaptable sensitivity and

limit of detection precisely response to a diverse range of concentrations in vitro. We expected the high adaptability of $Cu_{SA}C_6N_6$ along with the intrinsic outstanding temporal and spatial resolution of light stimuli, would supply a prospective candidate for dynamic analysis for intelligent artificial devices, such as robots, brain-machine interface, and internet-to-things in the future.

Conflict of interest

The authors declare no conflict of interest.

References

1. Johnson, D. G.; Hayward, J. S.; Jacobs, T. P.; Collis, M. L.; Eckerson, J. D.; Williams, R. H., Plasma norepinephrine responses of man in cold water. *J. Appl. Phycol.* **1977,** *43*, 216-220.

2. Cao, Z.; Livoti, E.; Losi, A.; Gärtner, W., A Blue Light-inducible Phosphodiesterase Activity in the Cyanobacterium Synechococcus elongatus. *Photochem. Photobiol.* **2010,** *86*, 606-611.

3. Wang, X. Q.; Chan, K. H.; Cheng, Y.; Ding, T.; Li, T.; Achavananthadith, S.; Ahmet, S.; Ho, J. S.; Ho, G. W., Somatosensory, Light-Driven, Thin-Film Robots Capable of Integrated Perception and Motility. *Adv. Mater.* **2020,** *32*, 2000351-2000360.

4. Wei, C.; Lin, W.; Liang, S.; Chen, M.; Zheng, Y.; Liao, X.; Chen, Z., An All-In-One Multifunctional Touch Sensor with Carbon-Based Gradient Resistance Elements. *Nano-Micro Letters* **2022,** *14*, 131.

5. Potyrailo, R. A., Multivariable Sensors for Ubiquitous Monitoring of Gases in the Era of Internet of Things and Industrial Internet. *Chem. Rev.* **2016,** *116*, 11877-11923.

6. Rudroff, F.; Mihovilovic, M. D.; Gröger, H.; Snajdrova, R.; Iding, H.; Bornscheuer, U. T., Opportunities and challenges for combining chemo- and biocatalysis. *Nat. Catal.* **2018,** *1*, 12-22.

7. Zhou, Z.; Zhang, Y.; Shen, Y.; Liu, S.; Zhang, Y., Molecular engineering of polymeric carbon nitride: advancing applications from photocatalysis to biosensing and more. *Chem. Soc. Rev.* **2018,** *47*, 2298-2321.

8. Fang, Y.; Hou, Y.; Fu, X.; Wang, X., Semiconducting Polymers for Oxygen Evolution Reaction under Light Illumination. *Chem. Rev.* **2022,** *122*, 4204-4256.

9. Bai, Y.; Zheng, Y.; Wang, Z.; Hong, Q.; Liu, S.; Shen, Y.; Zhang, Y., Metal-doped carbon nitrides: synthesis, structure and applications. *New J. Chem.* **2021,** *45*, 11876-11892.

10.   Yang, H.; Wang, Z.; Liu, S.; Shen, Y.; Zhang, Y., Molecular engineering

of CxNy: Topologies, electronic structures and multidisciplinary applications. *Chin. Chem. Lett.* **2020,** *31*, 3047-3054.

11. Yang, H.; Zhou, Q.; Fang, Z.; Li, W.; Zheng, Y.; Ma, J.; Wang, Z.; Zhao, L.; Liu, S.; Shen, Y.; Zhang, Y., Carbon nitride of five-membered rings with low optical bandgap for photoelectrochemical biosensing. *Chem* **2021,** *7*, 2708-2721.

12. Ma, J.; Peng, X.; Zhou, Z.; Yang, H.; Wu, K.; Fang, Z.; Han, D.; Fang, Y.; Liu, S.; Shen, Y.; Zhang, Y., Extended Conjugation Tuning Carbon Nitride for Non-sacrificial H_2O_2 Photosynthesis and Hypoxic Tumor Therapy. *Angew. Chem. Int. Ed.* **2022,** *61*, 202210856-202210865.

13. Mahmood, J.; Lee, E. K.; Jung, M.; Shin, D.; Jeon, I.-Y.; Jung, S.-M.; Choi, H.-J.; Seo, J.-M.; Bae, S.-Y.; Sohn, S.-D.; Park, N.; Oh, J. H.; Shin, H.-J.; Baek, J.-B., Nitrogenated holey two-dimensional structures. *Nat. Commun.* **2015,** *6*, 6486-6493.

14. Han, D.; Yang, H.; Zhou, Z.; Wu, K.; Ma, J.; Fang, Y.; Hong, Q.; Xi, G.; Liu, S.; Shen, Y.; Zhang, Y., Photoelectron Storages in Functionalized Carbon Nitrides for Colorimetric Sensing of Oxygen. *ACS Sens.* **2022,** *7*, 2328-2337.

15. Zhang, T.; Zhang, D.; Han, X.; Dong, T.; Guo, X.; Song, C.; Si, R.; Liu, W.; Liu, Y.; Zhao, Z., Preassembly Strategy To Fabricate Porous Hollow Carbonitride Spheres Inlaid with Single Cu–N_3 Sites for Selective Oxidation of Benzene to Phenol. *J. Am. Chem. Soc.* **2018,** *140*, 16936-16940.

16. Cai, J.; Huang, J.; Wang, S.; Iocozzia, J.; Sun, Z.; Sun, J.; Yang, Y.; Lai, Y.; Lin, Z., Crafting Mussel-Inspired Metal Nanoparticle-Decorated Ultrathin Graphitic Carbon Nitride for the Degradation of Chemical Pollutants and Production of Chemical Resources. *Adv. Mater.* **2019,** *31*, 1806314-1806325.

17. Liang, Y.; Xu, W.; Fang, J.; Liu, Z.; Chen, D.; Pan, T.; Yu, Y.; Fang, Z., Highly dispersed bismuth oxide quantum dots/graphite carbon nitride nanosheets heterojunctions for visible light photocatalytic redox degradation of environmental pollutants. *Appl. Catal. B-environ* **2021,** *295*, 120279-120291.

18. Huang, C.; Wen, Y.; Ma, J.; Dong, D.; Shen, Y.; Liu, S.; Ma, H.;

Zhang, Y., Unraveling fundamental active units in carbon nitride for photocatalytic oxidation reactions. *Nat. Commun.* **2021,** *12*, 320-328.

19. Fan, K.; Xi, J.; Fan, L.; Wang, P.; Zhu, C.; Tang, Y.; Xu, X.; Liang, M.; Jiang, B.; Yan, X.; Gao, L., In vivo guiding nitrogen-doped carbon nanozyme for tumor catalytic therapy. *Nat. Commun.* **2018,** *9*, 1440 -1451.

20. Zhou, Q.; Yang, H.; Chen, X.; Xu, Y.; Han, D.; Zhou, S.; Liu, S.; Shen, Y.; Zhang, Y., Cascaded Nanozyme System with High Reaction Selectivity by Substrate Screening and Channeling in a Microfluidic Device. *Angew. Chem. Int. Ed.* **2021,** *61*, 202112453-202112459.

21. Zhang, P.; Sun, D.; Cho, A.; Weon, S.; Lee, S.; Lee, J.; Han, J. W.; Kim, D.-P.; Choi, W., Modified carbon nitride nanozyme as bifunctional glucose oxidase-peroxidase for metal-free bioinspired cascade photocatalysis. *Nat. Commun.* **2019,** *10*, 940-954.

22. Vázquez-González, M.; Liao, W.-C.; Cazelles, R.; Wang, S.; Yu, X.; Gutkin, V.; Willner, I., Mimicking Horseradish Peroxidase Functions Using Cu^{2+}-Modified Carbon Nitride Nanoparticles or Cu^{2+}-Modified Carbon Dots as Heterogeneous Catalysts. *ACS Nano* **2017,** *11*, 3247-3253.

23. Ju, E.; Dong, K.; Chen, Z.; Liu, Z.; Liu, C.; Huang, Y.; Wang, Z.; Pu, F.; Ren, J.; Qu, X., Copper(II)-Graphitic Carbon Nitride Triggered Synergy: Improved ROS Generation and Reduced Glutathione Levels for Enhanced Photodynamic Therapy. *Angew. Chem. Int. Ed.* **2016,** *55*, 11467-11471.

24. Wu, Y.; Wu, J.; Jiao, L.; Xu, W.; Wang, H.; Wei, X.; Gu, W.; Ren, G.; Zhang, N.; Zhang, Q.; Huang, L.; Gu, L.; Zhu, C., Cascade Reaction System Integrating Single-Atom Nanozymes with Abundant Cu Sites for Enhanced Biosensing. *Anal. Chem.* **2020,** *92*, 3373-3379.

25. Wu, W.; Huang, L.; Wang, E.; Dong, S., Atomic engineering of single-atom nanozymes for enzyme-like catalysis. *Chem. Sci.* **2020,** *11*, 9741-9756.

26. Chen, X.; Zhao, L.; Wu, K.; Yang, H.; Zhou, Q.; Xu, Y.; Zheng, Y.; Shen, Y.; Liu, S.; Zhang, Y., Bound oxygen-atom transfer endows peroxidase-mimic

M–N–C with high substrate selectivity. *Chem. Sci.* **2021,** *12*, 8865-8871.

27.   Ji, S.;   Jiang, B.;   Hao, H.;   Chen, Y.;   Dong, J.;   Mao, Y.;   Zhang, Z.; Gao, R.;   Chen, W.;   Zhang, R.;   Liang, Q.;   Li, H.;   Liu, S.;   Wang, Y.;   Zhang, Q.;   Gu, L.;   Duan, D.;   Liang, M.;   Wang, D.;   Yan, X.; Li, Y., Matching the kinetics of natural enzymes with a single-atom iron nanozyme. *Nat. Catal.* **2021,** *4*, 407-417.

28.   Zhang, R.;   Xue, B.;   Tao, Y.;   Zhao, H.;   Zhang, Z.;   Wang, X.;   Zhou, X.;   Jiang, B.;   Yang, Z.;   Yan, X.; Fan, K., Edge-Site Engineering of Defective Fe–N_4 Nanozymes with Boosted Catalase-Like Performance for Retinal Vasculopathies. *Adv. Mater.* **2022,** *34*, 202205324-202205337.

29.   Wang, H.;   Jiang, D.;   Huang, D.;   Zeng, G.;   Xu, P.;   Lai, C.;   Chen, M.;   Cheng, M.;   Zhang, C.; Wang, Z., Covalent triazine frameworks for carbon dioxide capture. *J. Mater. Chem. A* **2019,** *7*, 22848-22870.

30.   Devautour-Vinot, S.;   Maurin, G.;   Serre, C.;   Horcajada, P.;   Paula da Cunha, D.;   Guillerm, V.;   de Souza Costa, E.;   Taulelle, F.; Martineau, C., Structure and Dynamics of the Functionalized MOF Type UiO-66(Zr): NMR and Dielectric Relaxation Spectroscopies Coupled with DFT Calculations. *Chem. Mater.* **2012,** *24*, 2168-2177.

31.   Zhu, X.;   Tian, C.;   Mahurin, S. M.;   Chai, S.-H.;   Wang, C.;   Brown, S.; Veith, G. M.;   Luo, H.;   Liu, H.; Dai, S., A Superacid-Catalyzed Synthesis of Porous Membranes Based on Triazine Frameworks for CO2 Separation. *J. Am. Chem. Soc.* **2012,** *134*, 10478-10484.

32.   Xiao, X.;   Gao, Y.;   Zhang, L.;   Zhang, J.;   Zhang, Q.;   Li, Q.;   Bao, H.; Zhou, J.;   Miao, S.;   Chen, N.;   Wang, J.;   Jiang, B.;   Tian, C.; Fu, H., A Promoted Charge Separation/Transfer System from Cu Single Atoms and C_3N_4 Layers for Efficient Photocatalysis. *Adv. Mater.* **2020,** *32*, 2003082-2003090.

33.   Sun, T.;   Li, Y.;   Cui, T.;   Xu, L.;   Wang, Y.-G.;   Chen, W.;   Zhang, P.; Zheng, T.;   Fu, X.;   Zhang, S.;   Zhang, Z.;   Wang, D.; Li, Y., Engineering of Coordination Environment and Multiscale Structure in Single-Site Copper Catalyst for

Superior Electrocatalytic Oxygen Reduction. *Nano Lett.* **2020,** *20*, 6206-6214.

34.   Yang, J.; Liu, W.; Xu, M.; Liu, X.; Qi, H.; Zhang, L.; Yang, X.; Niu, S.; Zhou, D.; Liu, Y.; Su, Y.; Li, J.-F.; Tian, Z.-Q.; Zhou, W.; Wang, A.; Zhang, T., Dynamic Behavior of Single-Atom Catalysts in Electrocatalysis: Identification of Cu-N3 as an Active Site for the Oxygen Reduction Reaction. *J. Am. Chem. Soc.* **2021,** *143*, 14530-14539.

35.   Zhang, L.; Long, R.; Zhang, Y.; Duan, D.; Xiong, Y.; Zhang, Y.; Bi, Y., Direct Observation of Dynamic Bond Evolution in Single-Atom Pt/C_3N_4 Catalysts. *Angew. Chem. Int. Ed.* **2020,** *59*, 6224-6229.

36.   Luo, L.; Gong, Z.; Xu, Y.; Ma, J.; Liu, H.; Xing, J.; Tang, J., Binary Au–Cu Reaction Sites Decorated ZnO for Selective Methane Oxidation to C1 Oxygenates with Nearly 100% Selectivity at Room Temperature. *J. Am. Chem. Soc.* **2021,** *144*, 740-750.

37.   Zhou, Y.; Zhang, L.; Wang, W., Direct functionalization of methane into ethanol over copper modified polymeric carbon nitride via photocatalysis. *Nat. Commun.* **2019,** *10*, 506-514.

38.   Ye, X.; Wang, X.; Kong, Y.; Dai, M.; Han, D.; Liu, Z., FRET Modulated Signaling: A Versatile Strategy to Construct Photoelectrochemical Microsensors for In Vivo Analysis. *Angew. Chem. Int. Ed.* **2021,** *133*, 11880-11884.

39.   Hong, Q.; Shen, Y.; Liu, S.; Zhang, Y., Re-Examination of Plotting Analytical Response against Different Forms of Concentration. *Anal. Chem.* **2021,** *93*, 11910-11914.

40.   Urban, P. L., Please Avoid Plotting Analytical Response against Logarithm of Concentration. *Anal. Chem.* **2020,** *92*, 10210-10212.